https://doi.org/10.26599/FRICT.2026.9441221

Research Article

Simultaneous measurement of normal and tangential forces on metal rough surfaces based on contact resistance

Xueqi Zhang [1, 2, 3], Wurui Ta[1, 2, 3, *], Hang Zhao [1, 2, 3], Youhe Zhou[1, 2, 3, *]

[1] Institute of Superconductor Mechanics, Lanzhou University, Lanzhou 730000, China

[2] Department of Mechanics and Engineering Science, College of Civil Engineering and Mechanics, Lanzhou University, Lanzhou 730000, China

[3] Key Laboratory of Mechanics on Environment and Disaster in Western China, The Ministry of Education of China, Lanzhou University, Lanzhou 730000, China

* Corresponding author, tawr@lzu.edu.cn, zhouyh@lzu.edu.cn

Received: October 11, 2025; Revised: December 16, 2025; Accepted: January 26, 2026

Abstract

Normal and tangential forces coexist between rough surfaces in engineering components under most operating conditions. Accurate measurement of contact forces (both normal and tangential forces) on rough surfaces is critical for the safety and stability of engineering equipment, as interfaces are typically discontinuous regions within mechanical systems. However, existing contact mechanics and electrical contact models mostly neglect tangential force effects, hindering their application to shearing behavior research and precluding the development of a contact force measurement methodology applicable to simultaneous normal and tangential force quantification. Inspired by the yield criterion for material damage, a contact mechanics model was developed that simultaneously accounts for the effects of normal and tangential forces. Then, a new principle of contact forces measurement is developed by correlating the contact resistance with the real contact area, which enables the simultaneous measurement of normal and tangential forces between rough surfaces based on the single contact resistance under steady-state contact conditions. By proposing a “static friction surface”, the static and dynamic friction stage is effectively differentiated, and the reasons for the sudden drop in friction force and the sudden increase in contact resistance during the static and dynamic transition stages are given. This work proposes a novel explanation for the friction mechanism in terms of mechanical deformation and electrical resistance changes.

Key words: rough surfaces; contact mechanic model; normal and tangential forces; contact resistance; synchronous measurement

1. Introduction

Due to the randomness and complexity of the roughness, multiple directional stresses are generated between the asperities when two rough surfaces are in contact. These multidirectional stresses can be synthesized macroscopically into normal and tangential (friction) forces (as shown in Fig. 1). Moreover, as sliding approaches between rough surfaces, the tangential force increases rapidly. Accurate measurement of contact normal and tangential forces on metallic rough surfaces is therefore critical, especially for mechanical engineering equipment, such as aircraft fuel line joint sealing surfaces [1], landing gear bearings and pancake superconducting coils, etc. This occurs because the assembly interfaces are often the discontinuous regions of the mechanical equipment, and thus constitute the weakest joints due to stress concentration. Therefore, understanding the state of contact forces at the rough assembly interface is critical for preventing serious structural failures in mechanical equipment. However, the complexity of the surface [2] severely limits the development of the contact mechanics models that can be analyzed for the simultaneous presence of normal and tangential forces, which makes the measurement of contact forces between rough contact surfaces remains highly challenging. In addition, the existence of adhesion [3] or wear phenomena also affects the development of electrical measurement methods.

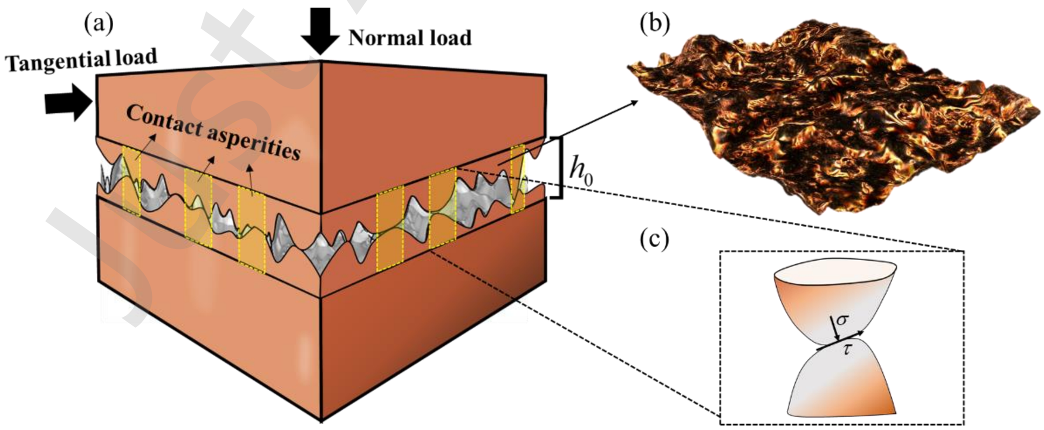

Fig. 1. (a) Schematic diagram of contact between rough surfaces under combined normal and tangential loads, h_0 is the initial height of contact surface; (b) Rough surface measured by ultra-depth three-dimensional microscope. (c) Schematic diagram of single pair of asperities under normal σ and shear stresses τ.

In order to accurately describe the contact properties of rough contact surfaces, the elastic contact theory of two-sphere contact was first proposed by Hertz [4], and the relationship between the indentation depth and the real contact area of the two spheres was studied. On this basis, scholars have developed a variety of classical rough surface contact models. Greenwood and Williamson [5] proposed the G-W model to reveal how the deformation of the contact interface changes with the topography of the surface. Based on this model, Greenwood and Tripp [6] describe the surface with a sphere of the same radius and a height that obeys a Gaussian distribution. Later, Greenwood and Tripp [7] extended the contact model from the contact between the rough surface and the plane to the contact between two rough surfaces, which solved the problem of mechanical action and geometric morphology that could not be considered in the previous model. Bush et al. [8] established a contact mechanics model by assuming that roughness occurs on many different length scales. Majumdar and Tien [9] introduced the W-M fractal geometry function into the characterization of surface roughness, and established a new characterization method of rough surface to characterize multi-scale self-affine surface. In addition, Persson [10,11,12] established a new contact model based on diffusion mechanisms, which is not only effective when the real contact area is smaller than the nominal contact area, but also particularly accurate when the extrusion force is large enough to be almost completely contacted within the nominal contact area. Persson et al. [13] extended their contact model to viscoelastic contact model. However, all these models seldom consider the role of tangential force, and an important reason is that many of them equate the contact between two rough surfaces as a contact between a rigid plane and an equivalent rough surface, which determines the mere normal force between the contacting surfaces without tangential force. This impedes the further application of existing contact mechanics models to shearing behavior studies, even though normal force and tangential force exist simultaneously between rough surfaces. More importantly, the limitations of these theoretical models fundamentally restrict its ability to form a contact forces measurement principle that can be applied to the measurement of contact forces (normal and tangential forces at the same time) at critical assembly interfaces in real mechanical engineering equipment.

In order to measure the contact forces between rough surfaces, a prerequisite is to identify a physical quantity sensitive to contact forces. Based on Holm's [14] and many scholars' research on electrical contact [15,16], it is known that the contact resistance is sensitive to normal force, so it is feasible to reflect the change of contact forces by contact resistance. The definition of contact resistance can be traced back to the electrical contact theory in 1941 [14]. Holm first gave the analytical expression of the contraction resistance according to the Laplace potential equation in the circular contraction zone of the ideal cylindrical conductor. Timsit [17] studied the shape of the isotropic equivalent contact point and the influence of the contraction zone on the contraction resistance. Greenwood [5] considered the actual contact characteristics of the rough interface, and proposed a contact resistance calculation formula based on a single cluster of contact points equivalent to multiple contact points of the interface without considering the size and distribution of the contact points. His calculation results are proved by Nakamura [18] and Minowa [19] using the finite element method and the Monte Carlo method, respectively. In addition, Lionel Boyer [20] introduced a shape factor to calculate the contact resistance of conductive spots with different shapes. Malucci [21] proposed a three-stage shrinkage model of contact resistance based on the characteristics of concentrated distribution of conductive spots at the contact interface and the influence of surface film on conductive spots. Ta et al. [22] proposed the concept of "real contact volume", which characterizes the contact behavior of rough surface through the ratio of void fraction and real contact volume, and further studies the effects of cyclic loading [23] and temperature [24] on the mechanical properties of interface contact. Based on the existing contact mechanics model and contact resistance model, scholars have established the electromechanical contact model of rough contact surface [25-31]. However, the existing electrical contact models are describing the contact forces variations by the existing contact mechanics models and still do not consider the effect of tangential force on the contact resistance. Therefore, although contact forces can be measured via contact resistance, the primary challenge lies in simultaneously measuring both normal and tangential forces from a single contact resistance signal. This necessitates establishing the relationship governing normal and tangential forces on rough surfaces.

In this paper, inspired by the yield criterion for material damage, the transition of rough surfaces from static to dynamic is considered as a form of interface damage. Based on this, the quantitative relation equations satisfied by the normal and tangential forces are proposed. Then, the real contact area is given from the geometric and mechanical equilibrium, respectively. Based on deformation compatibility, a system of equations governing normal and tangential forces is derived by equating the real contact areas. Finally, by relating the contact resistance to the real contact area, the “contact force-resistance” theoretical model is obtained, which contains three equations and three unknown quantities (normal force, tangential force and contact resistance). This forms a new principle of simultaneous measurement of normal and tangential forces based on the single contact resistance under steady-state contact conditions.

2. Electrical contact model under combined normal and tangential loads

Under a given normal load, the static friction force balances the applied tangential load until this force overcomes the maximum static friction. The maximum static friction force equals the product of the normal load and the static coefficient of friction. However, the relationship governing normal and tangential forces prior to the transition from static to dynamic friction remains unclear.

2.1. Relationship between normal and shear stresses

Normal and shear stresses at contacting asperities remain in equilibrium until sliding initiates, at which point the shear stress exceeds a critical value and disrupts this equilibrium. Inspired by the stress yield criterion for material damage, we treat slip between contacting asperities or rough surfaces as a damage mechanism. (as shown in Fig. 2(a), and the relationship between normal and shear stresses σ, τ on the asperities that satisfy a similar yielding criterion is as follows:

$$\sigma^2 + \eta\tau^2 = \sigma_Y{}^2 , \tag{1}$$

where, σ_Y is the yield stress of the material, η is a parameter related to material properties, which

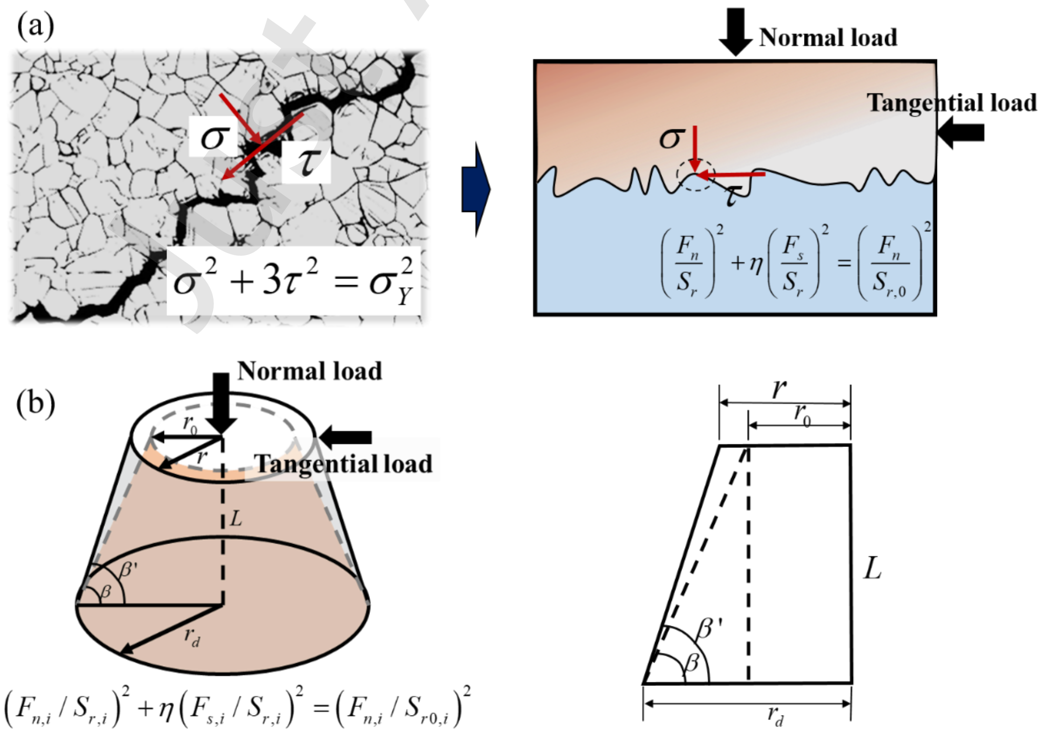

Fig. 2. (a) Inspired by the yield criterion for material fracture, the transition of the interface from static to dynamic is considered as the damage of the interface, the coefficient η is assumed to be a constant determined by material; (b)The deformation process of single asperity under combined normal and tangential loads and the contact radius and contact bottom angle have both increased under the action of tangential load.

can be measured experimentally. Then, the deformation of the contacting asperities consistent satisfy

$$\left(\frac{F_{n,i}}{S_{r,i}}\right)^2 + \eta\left(\frac{F_{s,i}}{S_{r,i}}\right)^2 = \left(\frac{F_{n,i}}{S_{r0,i}}\right)^2, \tag{2}$$

where, $F_{n,i}$ and $F_{s,i}$ are the normal and tangential forces on the contact surfaces of a single pair of asperities, respectively. $S_{r,i}$ is the real contact area of a single pair of asperities under the combined action of the normal and tangential forces, and $S_{r0,i}$ is the real contact area under the action of the normal force only. For the entire rough contact surfaces, the normal and tangential forces will also satisfy the

$$\left(\frac{F_n}{S_r}\right)^2 + \eta\left(\frac{F_s}{S_r}\right)^2 = \left(\frac{F_n}{S_{r,0}}\right)^2, \tag{3}$$

where, $F_n = \sum_{i=1}^{n} F_{n,i}$, $F_s = \sum_{i=1}^{n} F_{s,i}$. S_r is the total real contact area under the combined action of the normal and tangential forces. $S_{r,0}$ is the total real contact area under the action of the normal force only. Based on our earlier proposed theoretical model of volumetric contact under normal force only [23], the real contact area can be expressed as $S_{r,0} = S_{r0,i} \times n(h^*) = \pi r^2 N_{\max} \int_{h^*}^{1} C\chi h^{*\chi-1} dh^*$. This expression means that the real contact area is equal to the area of each pair of asperities multiplied by the number of contact points conforming to a probability distribution. which reflects the randomness of the contact process on rough surfaces.

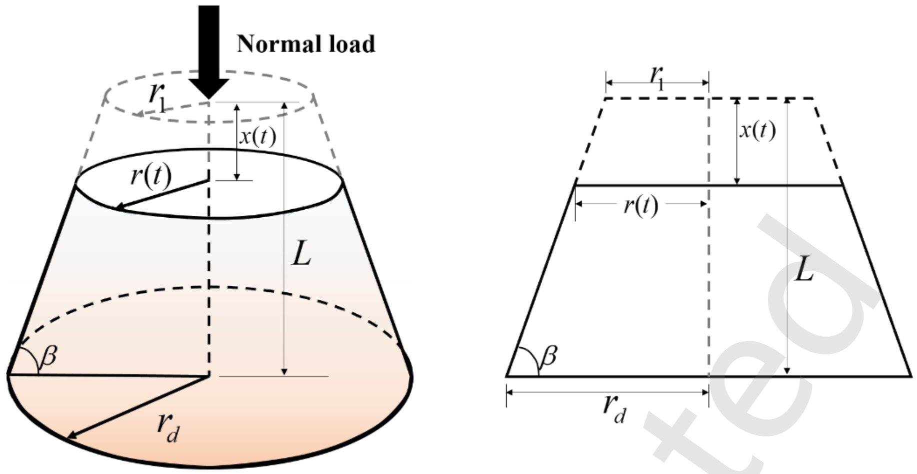

Fig. 3. Creep deformation model of a single asperity under the normal load. The normal compression amount is $x(t)$ and the contact radius $r(t)$ changes over time.

2.2. Creep constitutive model for contacting asperities

To calculate the area of a single pair of asperities in contact $S_{r0,i}$, we must determine how a single pair deforms under load. We consider that the asperity geometry on metal surfaces more closely approximates a frustum shape rather than the spherical description in Hertzian contact, and that the deformation process is analogous to a creep process. Therefore, the following creep constitutive relation is adopted to characterize the deformation of asperities [32]:

$$\dot{\varepsilon} = J\sigma^{p} e^{(-Q_c/KT)}, \tag{4}$$

where, $\dot{\varepsilon}$ is the creep rate, J is a constant, depending on the material and creep mechanism, σ is the normal stress, p is the stress index, Q_c is the creep activation energy, K is the Boltzmann constant, T is the temperature.

Based on the geometric relations of asperities (as shown in Fig. 3), the normal creep rate, normal stress, and contact radius of a contacting asperity can be expressed sequentially as

$$\dot{\varepsilon}(t)=\frac{\dot{x}(t)}{L},\ \sigma=\frac{F_i}{\pi r^2(t)},\ r(t)=\frac{\dot{x}(t)}{\tan(\beta)}, \tag{5}$$

where, $x(t)$ is the height variation of the asperity due to creep, L is the initial asperity height, F_i is the normal load on a single asperity, r is the asperity contact radius, β is the bottom inclination of the asperity. The geometric model dimensions represent averaged parameters (e.g., contact radius and asperity height). Combining equations (4) and (5) yields the following expression for the radius of the contact surface:

$$r(t)=\left(\frac{LJe^{(-Q_c/KT)}F_i^{\,p}(1+2p)}{\pi^p\tan(\beta)}\right)^{1/(1+2p)}t^{1/(1+2p)}, \tag{6}$$

Consequently, the real contact area of a single asperity under creep-dominated deformation is derived as

$$S_{r0,i}=\pi r^2=\pi A^2 t^{2\alpha}, \tag{7}$$

where, parameters A and α are expressed as

$$A=\left(\frac{LJe^{(-Q_c/KT)}F_i^{\,p}(1+2p)}{\pi^p\tan(\beta)}\right)^{1/(1+2p)},\ \alpha=\frac{1}{1+2p}, \tag{8}$$

Then, the expression for the real contact area under the combined effect of normal and tangential forces can be obtained from equation (3) as follows

$$S_r=S_{r,0}\sqrt{1+\eta\left(\frac{F_s}{F_n}\right)^2}=n\pi A^2 t^{2\alpha}\sqrt{1+\eta\left(\frac{F_s}{F_n}\right)^2}. \tag{9}$$

Equation (9) reveals the role of tangential force on the contact area, i.e., the mutual coupling of normal and tangential forces makes the contact area increase.

2.3. Geometric deformation equation

Although Equation (9) gives a relationship between normal and tangential forces that ensures the balance of forces in the static friction state, it cannot ensure deformation compatibility under combined normal and tangential loading. Therefore, deformation compatibility conditions must also be established from a geometric perspective. From the geometrical deformation of a pair of contacting asperities (e.g., Fig. 2(b)), the geometrical relations are satisfied after shear action as follows

$$\frac{r_d - r_0}{2}\tan\beta = \frac{r_d - r}{2}\tan\beta', \tag{10}$$

where, r_d is the radius of the bottom of the asperity, r_0, β is the contact radius and bottom inclination under the action of the normal force only, r, β' is the contact radius and bottom inclination under the combined action of the normal and tangential forces. Thus, the contact area can also be expressed as

$$S_r^{'} = n\pi r^2 = n\pi\left(r_d - \frac{\tan\beta}{\tan\beta'}\left(r_d - r_0\right)\right)^2, \tag{11}$$

In order to ensure that the deformations are coordinated, it is necessary to make $S_r = S_r^{'}$. Combined with $\tau_r = G\gamma = G(\beta' - \beta) = G\left[\arctan\frac{(r_d - r_0)\tan\beta}{(r_d - r)} - \beta\right]$ and $F_s = \tau_r S_r$, the final system of equations can be obtained as follows

$$\begin{cases} \pi\left(r_d - \dfrac{\tan\beta}{\tan\beta'}\left(r_d - At^{\alpha}\right)\right)^2 - \pi A^2 t^{2\alpha}\sqrt{1+\eta\left(\dfrac{F_s}{F_n}\right)^2} = 0 \\ F_s - G\pi\left(r_d - \dfrac{\tan\beta}{\tan\beta'}\left(r_d - At^{\alpha}\right)\right)^2\left[\arctan\dfrac{(r_d - r_0)\tan\beta}{(r_d - r)} - \beta\right] = 0 \end{cases}. \tag{12}$$

Now, the relationships governing normal and tangential forces at rough contact surfaces are established through contact forces equilibrium in the static friction phase, and geometric deformation coordination, respectively. Equation (12) contains two equations and two unknown variables (normal force and tangential force), the remaining parameters are either directly measurable or can be determined through established methods, which allows us to calculate the normal and tangential forces. Moreover, it is found that the variation of the real contact area is the bridge to correlate the normal and tangential forces and the most critical factor to reveal the contact behavior of rough surfaces.

2.4. Contact resistance under combined normal and tangential loads

When current flows through a rough metal interface, it is constricted to the real contact area, giving rise to contact resistance due to the constriction of current paths. Therefore, the value of the contact resistance directly reflects the change in the real contact area, which in turn reflects the change in contact force. Based on our previous work [22], the contact resistance R_c between rough interfaces can be considered as a parallel connection of the resistance R_i between many contacting asperities, which can be expressed as

$$\frac{1}{R_c} = \sum_{i=1}^{N} \frac{1}{R_i} = \sum_{i=1}^{N} \frac{S_i}{\rho L'} = \frac{S_r}{\rho L'}, \tag{13}$$

where, $L' = 2(L - At^{\alpha} \tan \beta)$ is the height of the asperity after deformation under normal and tangential forces. Thus, the total contact resistance between rough surfaces is as follows

$$R_c = \frac{\rho L'}{S_r} = \frac{2\rho(L - At^{\alpha} \tan \beta)}{S_{r,0}\sqrt{1+\eta\left(\frac{F_s}{F_n}\right)^2}}, \tag{14}$$

Now, a new set of equations is formed from equations (12) and (14) containing three independent equations and three unknown quantities (normal force, tangential force and contact resistance) as follows

$$\begin{cases} \pi\left(r_d - \frac{\tan\beta}{\tan\beta'}\left(r_d - At^{\alpha}\right)\right)^2 - \pi A^2 t^{2\alpha}\sqrt{1+\eta\left(\frac{F_s}{F_n}\right)^2} = 0 \\ F_s - G\pi\left(r_d - \frac{\tan\beta}{\tan\beta'}\left(r_d - At^{\alpha}\right)\right)^2\left[\arctan\frac{(r_d - r_0)\tan\beta}{(r_d - r)} - \beta\right] = 0. \\ R_c - \frac{2\rho(L - At^{\alpha}\tan\beta)}{S_{r,0}\sqrt{1+\eta\left(\frac{F_s}{F_n}\right)^2}} = 0 \end{cases} \tag{15}$$

This system of equations (15) allows us to calculate the value of the interfacial contact resistance under normal and tangential forces. Conversely, the normal and tangential forces can be calculated from the actual measured contact resistance value, i.e., simultaneous measurement of the two quantities, normal and tangential forces, by means of the single contact resistance under steady-state contact conditions.

3. Experimental validation of the electrical contact model

To validate the proposed model, we conducted contact resistance measurements on metal specimens subjected to the combined effects of normal and tangential loads. Stainless steel was chosen as the experimental specimen for its exceptional corrosion resistance and high strength properties that also lead to its broad industrial applicability (as shown in Fig. 4(a)). And an apparatus was constructed to measure variations in tangential loads and electrical signals during frictional sliding under controlled normal loads (as shown in Fig. 4(b) and 4(c)). Tangential loads at the interface were obtained from the displacement of a force transducer (stiffness: 453 N/mm). The contact resistance was measured using the four-wire method and the electrical data were recorded and analyzed via an M81 synchronous source-measure unit (SSM). The experimental apparatus comprised direct shear device, M81 SSM system, loading mechanism and wires.

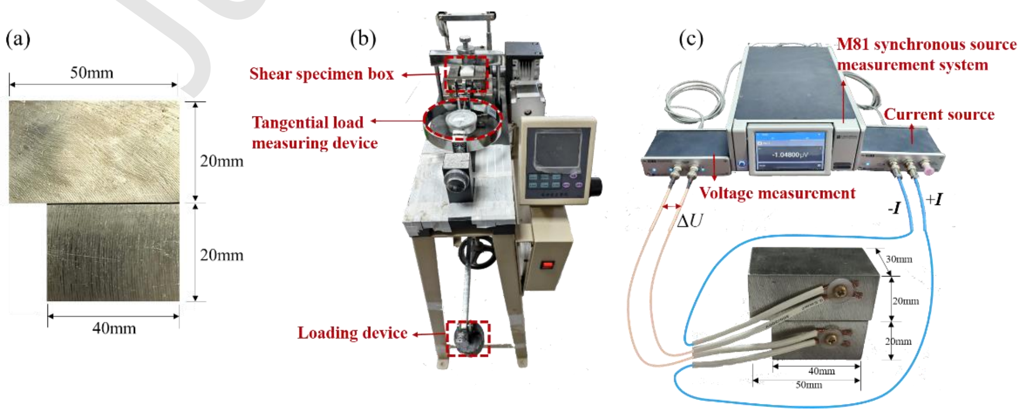

Fig. 4. (a) Diagram of specimen dimensions; (b) The apparatus of normal and tangential forces loading

for rough interfaces; (c) M81 synchronous source measurement system and contact resistance measurement principle.

3.1. Experimental procedure

To measure the contact resistance under different normal and tangential loads, the metal specimens was first mounted in the loading mechanism. The normal load was gradually increased without applying tangential load while measuring the contact resistance, in order to investigate the creep behavior of the interface and the influence of normal load on contact resistance. In the second step, under constant normal load, tangential load was applied while the contact resistance was measured simultaneously. This process was repeated multiple times to obtain reliable contact resistance data under varying normal and tangential load conditions. The normal loading device provided a force range of 0–1000 N, and the SSM instrument supplied a direct current of 0.1 A, to maintain environmental stability and interfacial consistency, all stainless-steel specimens underwent standardized pretreatment before testing: Surface contaminants (dust, oils) were removed by wiping with filter paper; Residual debris was eliminated via 3–5 minutes of compressed air blowing; This protocol ensured consistent surface roughness across specimens.

3.2. Comparison of theoretical and experimental results

Firstly, the electrical contact characteristics of the material under normal load are verified. All parameter values used in the calculations are provided in Table 1.

Table 1. Determination of model calculation parameters

Parameter	Value

Roughness parameter χ, C	3, 0.82
Stress index, p [33]	4.2
Initial asperity height, L	4×10^{-6} m
Bottom inclination, β	pi/4 rad
Asperity radius of bottom, r_d	6×10^{-6} m
Material creep parameters, J [33]	9×10^{-6}
Creep activation energy, Q_c	3×10^{-19} J
Boltzmann constant, K	1.380649×10^{-23} J/K
Resistivity (stainless steel), ρ	7.3×10^{-7} Ω·m
Material parameter, η	400
Shear modulus, G	1×10^{11} Pa

As shown in Fig. 5(a), the contact resistance measured by the experiment shows a nonlinear decreasing trend with the stepwise increase of the normal load. A distinct plastic creep process was observed during the application of normal load, confirming the validity of the selected creep model describing deformation of asperities. Fig. 5(b) shows the relationship between the normal load and the contact resistance given by the theoretical model and the comparison of the experimental values. The error between the theory and the experiment is within 7%, which proves the accuracy of the theoretical model.

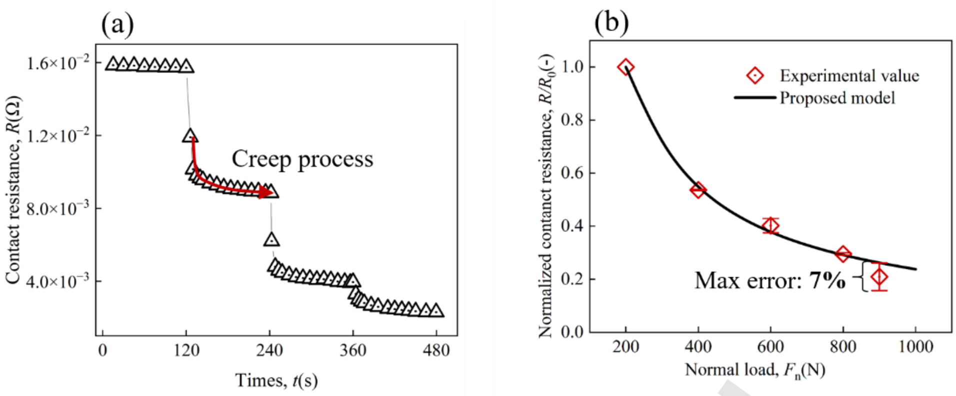

Fig. 5. (a) The variation of contact resistance with time under different normal loads; (b) The relationship between normalized contact resistance and normal load, theoretical and experimental results.

Next, the contact model and experimental results under the simultaneous action of normal and tangential loads are verified. Firstly, the influence of contact forces on shear strain and real contact area is considered. Fig. 6(a) shows the comparison between the theoretical prediction results of the relationship between tangential strain and tangential load and the experimental measurement data. The comparison shows good agreement, with a maximum error of 12%, confirming the validity of the proposed model in predicting shear strain. Fig. 6(b) presents experimental results showing the variation of real contact area with tangential load. As observed, the real contact area increases linearly with increasing tangential load. This trend demonstrates that tangential load influences contact resistance by altering the real contact area, thus validating the correctness of employing the electrical measurement method for measuring contact forces.

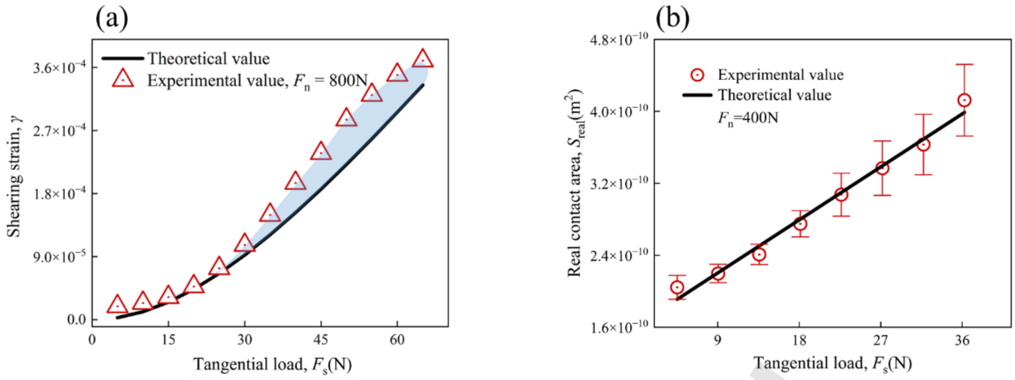

Fig. 6. (a) Comparison between theoretical and experimental results of the shear strain versus tangential load under 800N normal load; (b) Comparison between theoretical and experimental results of the real contact area versus tangential load under 400N normal load.

The variation of real contact resistance with contact force under normal load and tangential load is considered respectively, as shown in Fig. 7. The contact area increases under both normal and tangential loads, thus decreasing the contact resistance due to reduced current constriction. Further loading of tangential load under normal load causes the contact resistance to decrease, due to the increase in contact area. Moreover, as the normal load increases, the maximum value of the tangential load that can be applied increases, i.e. the more tangential load is required for sliding. The above model prediction results are in good agreement with the experimental results, indicating that the proposed model can well reflect the relationship between the interface contact resistance and the interface contact force, and provide theoretical support for the subsequent measurement methods.

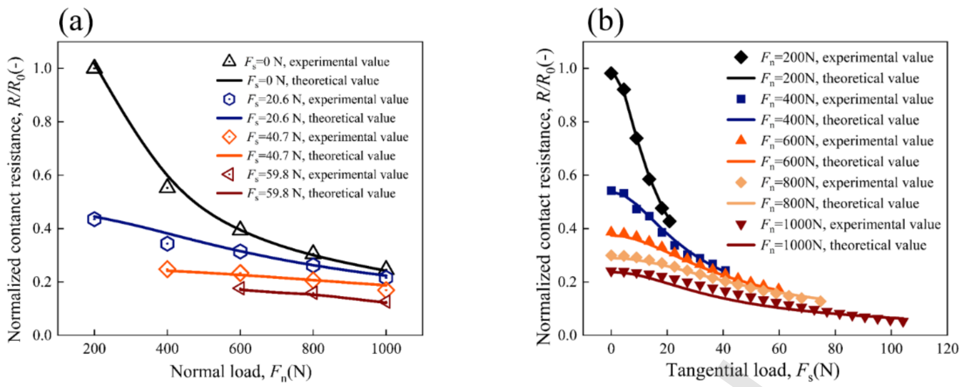

Fig. 7. (a) The comparison results of theoretical and experimental values of normalized contact resistance and normal load at different tangential loads; (b) The comparison results of theoretical and experimental values of normalized contact resistance and tangential load at different normal loads.

4. Synchronous measurement of normal and tangential forces based on contact resistance

After validating the aforementioned model, we can proceed to simultaneous measurement of normal and tangential forces using a single contact resistance value under steady-state contact conditions. In practical applications, however, we cannot know beforehand whether a tangential force exists. Therefore, when a resistance value is measured, we must first determine whether a tangential force is present. Based on this determination, we then proceed to calculate the normal and tangential forces.

4.1. Determining the existence of tangential force

The judgment procedure is outlined as follows. Firstly, we measured the contact resistance R_{c0}, and assumed the tangential force F_s is zero. Then this condition $F_s = 0$ is substituted into the geometric deformation equation (12) to solve for the normal force F_{n1}. Subsequently, both $F_s = 0$ and F_{n1} are substituted into the equation (14) to calculate the corresponding contact resistance R_{c1}.

The values of R_{c0} and R_{c1} are then compared. If $R_{c0} \geq R_{c1}$, it is concluded that no tangential force is present, and F_{n1} represents the normal force. If $R_{c0} < R_{c1}$, the measured contact resistance R_{c0} is substituted into the electrical measurement equation system (15) to determine both the normal force F_{n2} and tangential forces F_{s2}. Fig. 8 shows the judgment process of whether the tangential force exists.

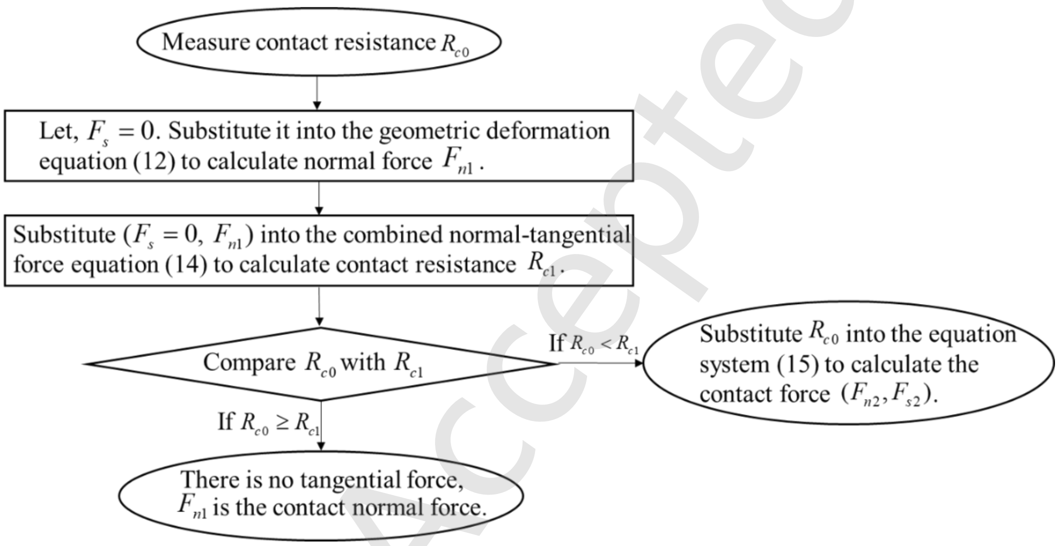

Fig. 8. Flowchart illustrating the procedure for determining the existence of tangential force.

This electrical measurement method proposed in this study effectively solves the multi solution problem of the relationship between contact resistance and contact force in the traditional model by introducing multiple physical field constraints composed of electrical, mechanical equilibrium, and geometric coordinate equations. And adopt a physics based decision-making process to uniquely determine the force state.

4.2. Simultaneous measurement of normal and tangential forces

According to the above procedure, if there are both normal and tangential forces present simultaneously and they remain unchanged, the measured contact resistance values were substituted into the system of equations (15) to calculate the contact forces. In order to validate the feasibility and accuracy of the proposed measurement method. These calculated values were then compared with the applied loads, the detailed computational procedure consisted of the following steps.

Firstly, the metal specimens were mounted in a combined normal-tangential testing apparatus, a predetermined normal load was applied, and a tangential load was subsequently introduced. During loading, a current was supplied to the specimen to determine the interfacial contact resistance. The normal and tangential forces were evaluated using the identification flowchart outlined in the previous section and subsequently compared to the experimentally applied loads. This procedure was repeated multiple times to ensure the reliability of the results

As shown in Fig. 9, the measured forces (solid points) obtained via the electrical method agree closely with the applied normal and tangential loads (hollow points), the maximum is 9.8%, confirming the feasibility and high accuracy of the proposed measurement technique.

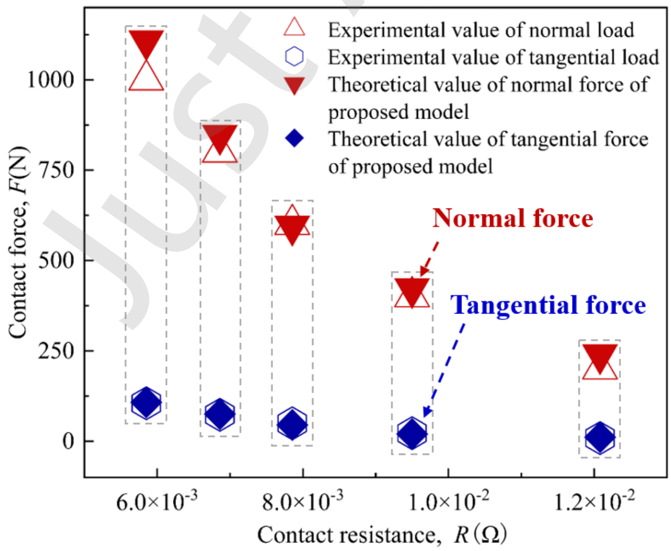

Fig. 9. Simultaneous measurement of normal and tangential loads on rough surfaces of stainless-steel specimens based on a single contact resistance.

The proposed electrical measurement method can achieve synchronous measurement of contact force through a single contact resistance under steady-state contact conditions. The key is to first determine the existence of tangential load through the decision-making process, and then substitute the contact resistance into a closed equation system that satisfies the mechanical equilibrium equation, deformation coordination equation, and electrical equation, providing a new perspective and method for measuring interface contact force.

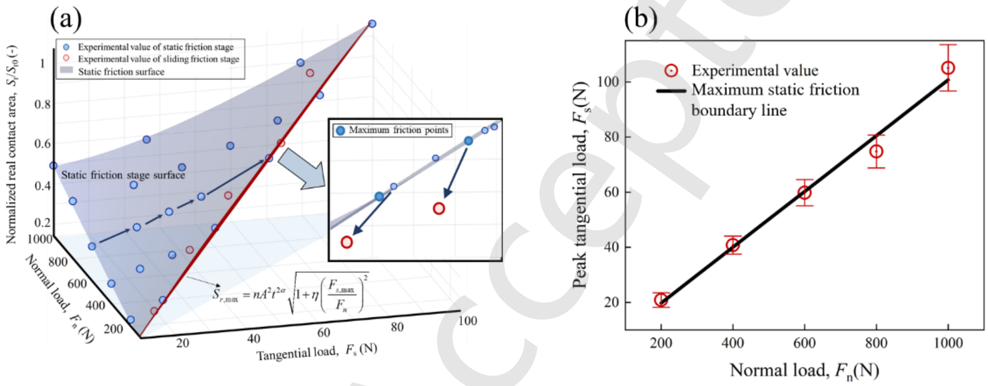

Fig. 10. (a) The "static friction surface" of a rough surface during normal and tangential loading, the contact relationship between the blue dot and the "static friction surface" distinguishes different friction stages; (b) The experimental value of peak tangential load and normal load and the boundary curve of maximum static friction force.

5. Static-dynamic friction transition mechanism

Based on observations of real contact area variations during the application of tangential load, a "static friction surface" and a new transition mechanism between static and dynamic friction are proposed, grounded in changes in the real contact area. In Fig. 10(a), the gray surface resembles the yield surface of material damage and is termed the "static friction surface", which satisfied the equation of $\left(\frac{F_n}{S_r}\right)^2+\eta\left(\frac{F_s}{S_r}\right)^2=\left(\frac{F_n}{S_{r,0}}\right)^2$. And the equation can be further expressed as $S_r=S_{r,0}\sqrt{1+\eta(\frac{F_s}{F_n})^2}$,which reflect the relationship between the real contact area and the normal load and the tangential load. The experimental values of real contact area are calculated by reverse calculation of the contact resistance. All points on this surface are in the static friction stage, which means that no matter how the normal and tangential loads vary, there is no sliding between the rough surfaces as long as they are on this surface. As the normal and tangential loads increase, the blue dots on the surface (real contact area) gradually move closer to the red line at the edge (maximum real contact area). When the red line is exceeded, sliding occurs between the rough surfaces and static friction transforms into dynamic friction. The reason for the existence of the boundary of the "static friction surface" is that the friction has the maximum static friction force. At this moment, the equilibrium state of static friction is broken and the interface deformation reaches its maximum value (maximum real contact area). The tangential load is momentarily reduced due to the interface destabilization, resulting in a reduction of the real contact area, which is similar to the unloading process. The red dots are the dynamic friction states, which are all below the static friction surface. Fig. 10(b) shows the relationship between the peak tangential load and the normal load. They satisfy the linear relationship, which proves the repeatability of the shear experiment and provides a demonstration for the parameter η as a constant. The black line in the figure is the red boundary line of Fig. 10(a), which represents the theoretical maximum static friction boundary.

This destabilization process explains why maximum static friction exceeds dynamic friction. The variable real contact area effectively characterizes static and dynamic friction states and their transition, replacing the conventional two-parameter description based on maximum static and dynamic friction coefficients. For a certain normal load, the real contact area increases with the tangential load. When it increases to a maximum value, the interface destabilizes and begins to slide, the real contact area decreases and soon reaches a stabilizing value, which will vary very little during the dynamic friction stage (as shown in Fig. 11).

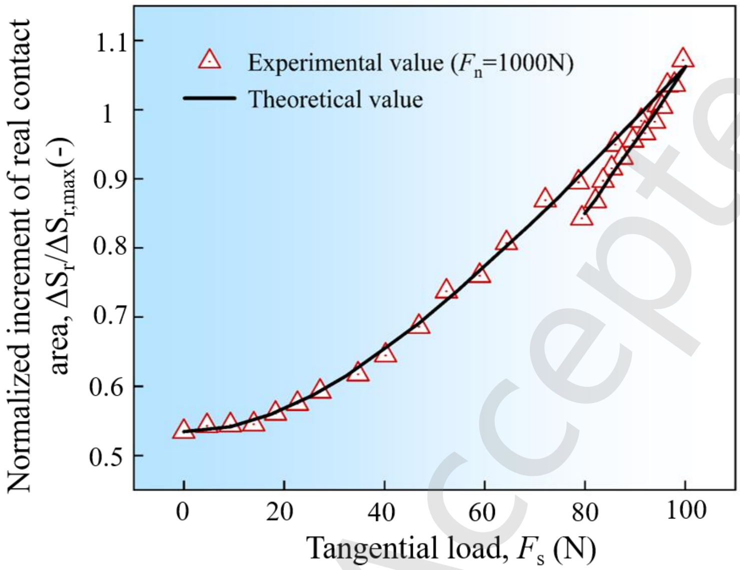

Fig. 11. The theoretical and experimental comparison between normalized real contact area increment and tangential load shows that after the tangential load reaches its maximum value, both the real contact area and tangential load decrease simultaneously.

Correspondingly, the curve of friction force with time will show a sudden drop in the static-dynamic transition stage, while the contact resistance will show a sudden increase in this stage (as shown in Fig. 12(a)). This is all due to the change in the real contact area. The maximum static friction coefficient corresponds to the maximum real contact area, while the dynamic friction coefficient corresponds to the real contact area after destabilization. This relationship is demonstrated in Fig. 12(b), where it can be seen that the ratio of the static and dynamic friction coefficients (μ_k / μ_s) and the ratio of the maximum real contact area to the contact area after destabilization ($S_{r,m} / S_{r,k}$) are almost equal. Therefore, the contact resistance curve can also accurately reflect the change in friction, which provides a new way of measuring friction forces.

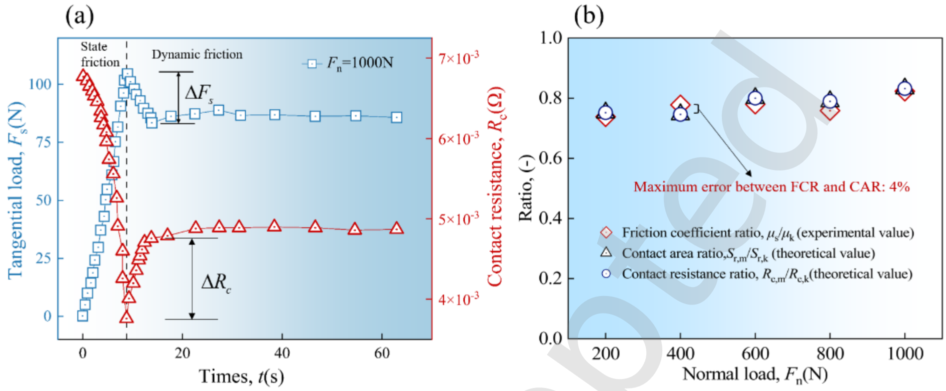

Fig. 12. (a) Simultaneous evolution curves of experimentally measured friction and contact resistance with time; (b) Comparison of the ratio of the real contact area in the static and dynamic phases with the ratio of the static and dynamic coefficients of friction.

6. The influence of temperature and roughness

The proposed model exhibits pronounced creep behavior and is therefore influenced by temperature variations. Additionally, it can effectively capture the effect of varying surface roughness levels on interfacial contact behavior. Fig.13 shows the variation of normalized real contact resistance with tangential load under different temperature conditions. It can be seen that the contact resistance decreases with the increase of temperature. This is due to the increase of creep rate caused by the change of temperature, which leads to the increase of real contact radius, that is, the increase of real contact area, which leads to the decrease of contact resistance.

Next, the effects of different asperity radius and roughness distribution on contact resistance were investigated respectively. Fig. 14(a) shows the variation of normalized real contact area with tangential load under different contact radius conditions. It can be seen that the influence of temperature on real contact resistance is consistent with the influence of contact radius on real contact resistance, which proves that the above analysis is reasonable. The Fig. 14(b) shows the schematic diagram of asperities with the same rough distribution and different contact radius.

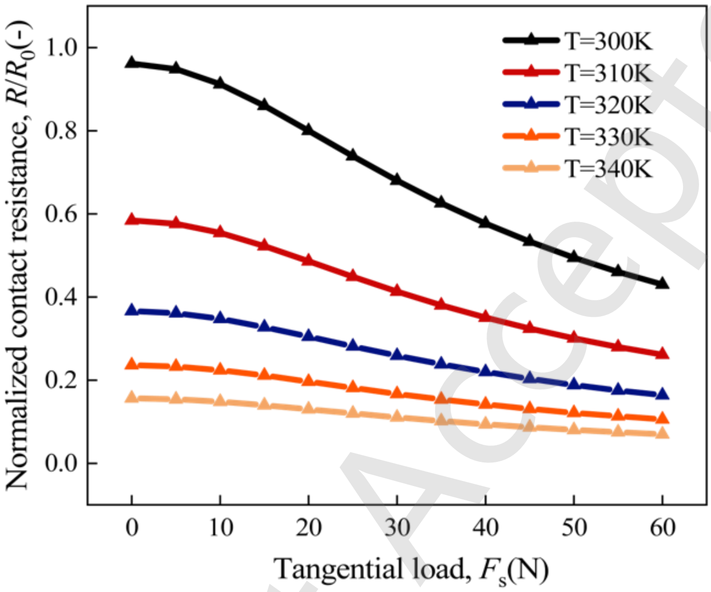

Fig. 13. The variation of normalized real contact resistance with tangential load at different temperatures under the 600N normal load.

Fig. 14(c) shows the variation of normalized real contact area with tangential load under different rough surface distribution conditions. The derivation of the interface roughness distribution is detailed in the references [23], the real contact number of rough contact interface satisfied $n(h^*) = N_{\max}\int_{h^*}^{1} B\chi h^{*\chi-1} dh^*$. It can be observed that as the roughness parameter χ increases, the real contact resistance exhibits a linearly decreasing trend. This occurs because the value of χ influences the distribution of asperities on the rough surface: a larger value of χ results in a greater number of real contact points. Furthermore, the homogenization approach adopted in the model causes the number of contact points to linearly affect the real contact area. The Fig. 14(d) shows the schematic diagram of asperities with the same contact radius and different rough distribution.

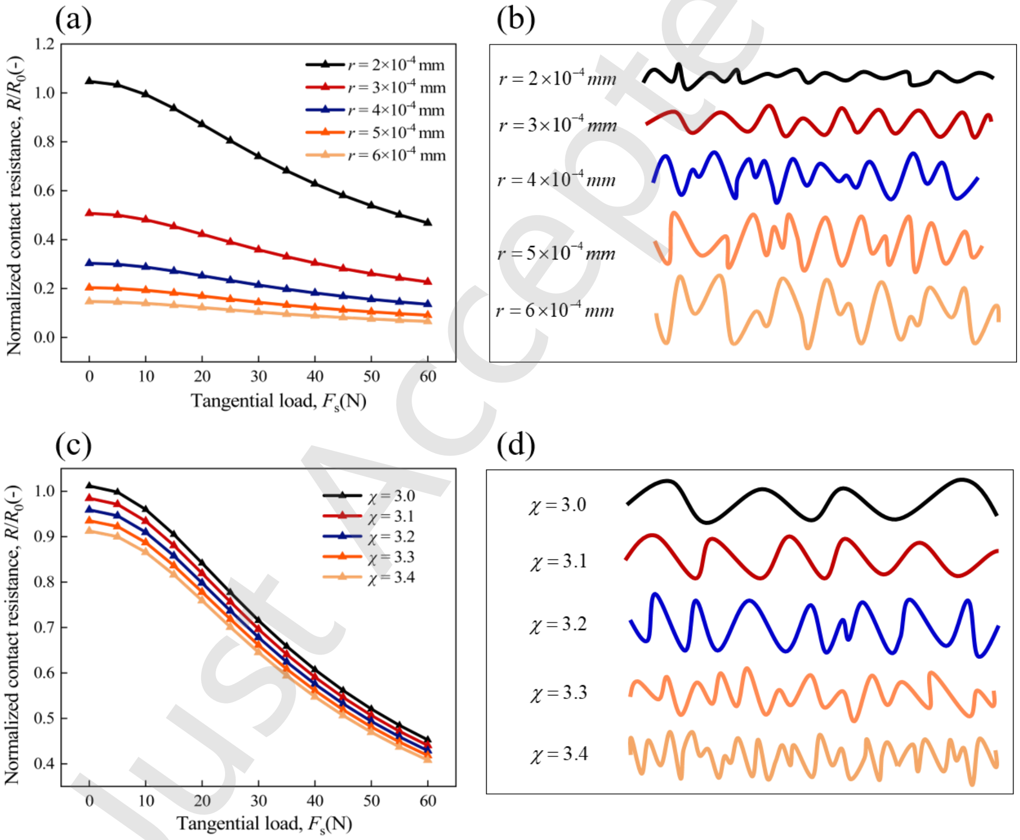

Fig. 14. (a) The variation of normalized real contact resistance with tangential load under different contact radii under the 600N normal load; (b) The schematic diagram of asperities with the same rough distribution and different contact radius; (c) The variation of normalized real contact resistance with tangential load under different distribution forms under the 600N normal load; (d) The schematic diagram of asperities with the same contact radius and different rough distribution.

7. Discussions

Above all, inspired by the yield criterion for material damage, a contact mechanics model is developed that simultaneously considers the effects of normal and tangential loads, which both satisfies mechanical equilibrium and ensures deformation coordination closing to the real situation. Compared with the traditional model, the proposed model, the new model reveals for the first time that tangential forces reduce contact resistance, as the tangential forces also increase the actual contact area. Then a new principle of contact force measurement is developed by correlating the contact resistance with the real contact area, which enables the simultaneous measurement of normal and tangential forces between rough surfaces based on the single contact resistance under steady-state contact conditions. Although rough surfaces are complex and random, we have revealed the mechanical mechanisms of static and dynamic friction by investigating the evolution of the real contact area. By proposing a “static friction surface”, the static and dynamic friction stage is effectively differentiated, and the reasons for the sudden drop in friction force and the sudden increase in contact resistance during the static and dynamic transition stages are explained, which is due to the evolution of the contact area. Finally, we considered the influence of temperature and roughness on contact resistance. The increase of temperature will lead to the decrease of contact resistance. And the change of roughness mainly affects the contact resistance from the contact radius and the roughness distribution. The increase of contact radius leads to the decrease of contact resistance, and the rougher surface also leads to lower contact resistance.

Although the model well reflects the contact force on metal contact problems under plastic and creep deformation conditions, there is still a lack of discussion on the adhesion, wear, and physicochemical effects that exist in practice. Therefore, it is necessary to extend the model under strong adhesion or severe wear conditions.

8. Conclusions

In summary, a novel electro-mechanical contact model has been established that simultaneously accounts for normal and tangential forces. This model reveals for the first time the influence of tangential force on contact resistance and explains the mechanism of static-dynamic transition in the friction process through contact area evolution. By identifying the presence or absence of tangential forces, it provides the capability to simultaneously measure both normal and tangential forces from a single contact resistance measurement under steady-state contact conditions. Furthermore, by proposing the "static friction surface" concept, we mechanistically explain friction force drops and resistance surges during static-dynamic transitions. Additionally, we discover that contact resistance tends to decrease with increasing roughness, attributed to changes in contact area and the number of contact points. The research has advanced the development of contact mechanics and electrical contact theory models, and provided a novel approach for measuring contact forces between rough surfaces based on contact resistance measurements, thereby establishing a methodological foundation for engineering applications.

Appendix A. Method for determining roughness parameters

Due to the high complexity and randomness of real surfaces, measurements of roughness parameters face significant challenges. In the preliminary work of our research team, the concept of contact volume was proposed to probabilistically characterize the random contact process of rough surfaces. The roughness of the rough surface affects the size of the contact asperity and the number of contact points. The roughness parameter χ, C used in this paper significantly affects the number of real contact points. Based on the preliminary work [23], we derived the relationship between the number of contact points and roughness parameters. The proportion of real contact volume γ is defined as follows

$$\gamma = V_{real} / V_{rough}, \tag{A-1}$$

Where, V_{real} is real contact volume, V_{rough} is rough volume.

$$\gamma V_{rough} = n V_{real-i}, \tag{A-2}$$

thus

$$N_{\max} = \frac{V_{real-\max}}{V_{real-i}} = \frac{S_n h_0 (1-\alpha_0)}{S_{real-i} h_0 (1-\alpha_0)} = \frac{S_n}{\pi R_0^{\ 2}}, \tag{A-3}$$

finally, γ can be expressed as

$$\gamma = \frac{V_{real}}{V_{rough}} = \frac{n}{N_{\max}}, \tag{A-4}$$

During the loading process, γ is obviously a function of interface porosity α, and the function of interface real contact points as porosity is obtained as follows

$$n(\alpha) = N_{\max} \int_{\alpha}^{1} \gamma'(\alpha) d\alpha, \tag{A-5}$$

As the variations in indentation depth induce changes in porosity, γ is considered a function of indentation depth h. In order to determine the probability density function $\gamma'(h)$. We analogize the change in the ratio of real contact area to nominal contact area during contact with a single rough surface support curve. The detailed parameter analogy relationships refer to reference [23]. Finally, the real contact points can be expressed as

$$n(h^*) = N_{\max} \int_{h^*}^{1} C \chi h^{*\chi-1} dh^*. \tag{A-6}$$

where, the $h^* = h_0 - d / h_0$, is the equivalent indentation depth; The χ, C is the roughness parameters, which can be obtained from the rough surface bearing area curve.

Appendix B. Calculation of real contact resistance

The experimentally measured total resistance consists of substrate resistance and contact resistance, therefore the real contact resistance is calculated by subtracting the substrate resistance from the total resistance. As the Fig. B1 shows, the rough contact volume is equivalent to contact blocks with heights of h_1 , h_2 . The relationship between total resistance, contact resistance, and substrate resistance is

$$\begin{cases} R_t^1 = R_b^1 + R_c^1 \\ R_t^2 = R_b^2 + R_c^2 \end{cases} \Rightarrow \begin{cases} \varphi_t^1 = \varphi_b^1 + \varphi_c^1 \\ \varphi_t^2 = \varphi_b^2 + \varphi_c^2 \end{cases}, \tag{B-1}$$

where, R_t is the total resistance, R_b is the substrate resistance, R_c is the contact resistance. The numbers 1 and 2 represent the upper and lower specimen blocks.

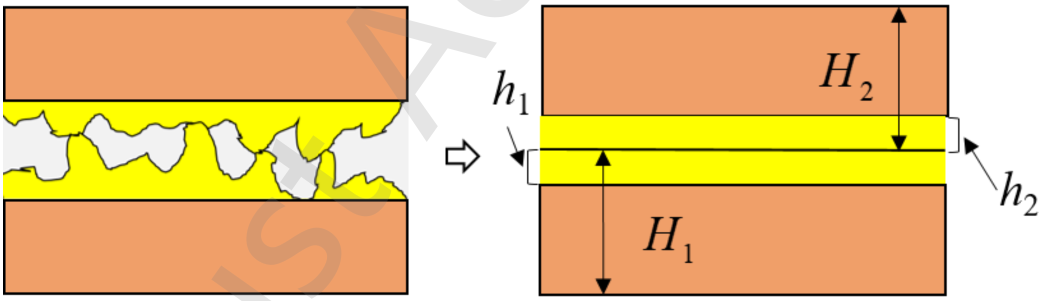

Figure. B1. Equivalent calculation model of real contact resistance and substrate resistance of rough contact surface; h_1 , h_2 represents the height of the equivalent contact block respectively and H_1 , H_2 represents the height of substrate blocks respectively.

The boundary condition for the total potential is

$$\begin{cases} \left.\dfrac{\partial \varphi_t^1}{\partial z_1}\right|_{z_1=0} = -\rho_1 J\left(x,y\right) \\ \left.\dfrac{\partial \varphi_t^1}{\partial z_1}\right|_{z_1=\infty} = -\rho_1 \overline{J} \end{cases} \quad \begin{cases} \left.\dfrac{\partial \varphi_t^2}{\partial z_2}\right|_{z_2=0} = -\rho_2 J\left(x,y\right) \\ \left.\dfrac{\partial \varphi_t^2}{\partial z_2}\right|_{z_2=\infty} = -\rho_2 \overline{J} \end{cases}, \tag{B-2}$$

where, ρ is the conductivity of specimens, z is the distance. If the contact interface is completely in contact, the boundary condition for the substrate potential is

$$\begin{cases} \left.\dfrac{\partial \varphi_b^1}{\partial z_1}\right|_{z_1=0} = -\rho_1 \overline{J} \\ \left.\dfrac{\partial \varphi_b^1}{\partial z_1}\right|_{z_1=\infty} = -\rho_1 \overline{J} \end{cases} \quad \begin{cases} \left.\dfrac{\partial \varphi_b^2}{\partial z_2}\right|_{z_2=0} = -\rho_2 \overline{J} \\ \left.\dfrac{\partial \varphi_b^2}{\partial z_2}\right|_{z_2=\infty} = -\rho_2 \overline{J} \end{cases}, \tag{B-3}$$

It can be deduced that the matrix potential is a function of z, that

$$\varphi(z) = Az + B, \tag{B-4}$$

According to boundary conditions

$$\left.\frac{\partial \varphi_b^1}{\partial z_1}\right|_{z_1=0} = -\rho_1 \overline{J} \quad A = -\rho^i \overline{J} \ \left(i = 1,2\right), \tag{B-5}$$

In the infinite region, z tends towards infinity, and the potential tends to 0, thus

$$B = 0, \quad \varphi(z) = -\rho^i \overline{J} z, (i = 1,2) \quad \overline{J} = I / LW, \tag{B-6}$$

where, L, W are the length and width of the specimens respectively. And the substrate resistance is

$$\begin{cases} R_b^1 = \varphi_1 / I = \rho^1 \dfrac{I}{LW}\left(H_1 - h_1\right)\dfrac{1}{I} = \rho^1 \dfrac{\left(H_1 - h_1\right)}{LW} \\ R_b^2 = \varphi_2 / I = \rho^2 \dfrac{I}{LW}\left(H_2 - h_2\right)\dfrac{1}{I} = \rho^2 \dfrac{\left(H_2 - h_2\right)}{LW} \end{cases}, \tag{B-7}$$

Finally, the real contact resistance obtained is

$$R_c = R_t - \rho \frac{\left(H_1 + H_2 - h_2 - h_1\right)}{LW}, \tag{B-8}$$

Appendix C. Surface morphology characterization and power spectral density analysis

In order to comprehensively characterize the rough surface, we conducted three-dimensional surface measurements on the specimens before and after the friction process (as shown in Fig. C1). To measure the surface morphology of the specimens before and after friction, a MicroXAM-800 non-contact optical profiler was employed to measure morphology and roughness. The spatial resolution is 0.1μm (X direction), 0.1μm (Y direction), and 0.1nm (Z direction), and the measurement is used a lens with a magnification of 5times.

As shown in Fig. C2 (a) and (c), on the original surface before friction, the contour of the asperity is sharp. After experiencing normal loading and tangential sliding (Fig. C2(c) and (d)), the peaks of these asperities showed significant local crushing and plastic flattening, manifested as a significant decrease in peak height and lateral expansion of the contact area. At the same time, the valley areas between the asperities have basically maintained their original morphology and have not undergone significant deformation. The typical feature of “peak deformation and valley floor invariance” provides direct experimental evidence for the classical contact theory that contact only occurs on the peak of some asperities, and verifies the basic assumption of the model in this paper that the overall contact is regarded as a set of independent asperities contacts.

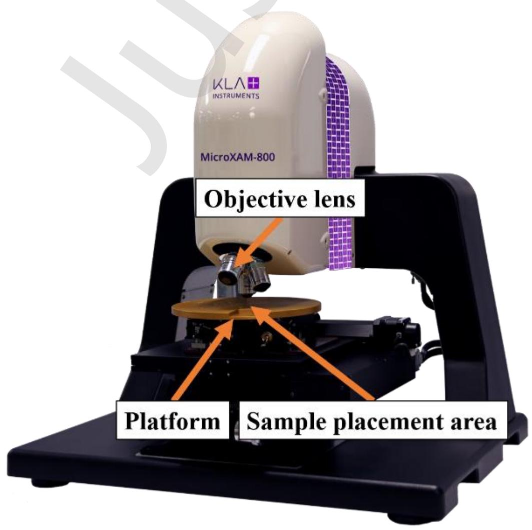

Figure. C1. MicroXAM-800 non-contact optical profiler.

The one-dimensional power spectral density (PSD) was calculated based on the surface height data obtained by ultra-depth 3D microscopy. First, the original data were preprocessed to remove tilt and noise. Then, a one-dimensional fast Fourier transform (1D FFT) was performed on the processed height matrix, and its power spectrum was calculated. Through statistical analysis of the spatial frequencies, the power spectral density curves characterizing the surface topography features were obtained (as shown in Fig. C3).

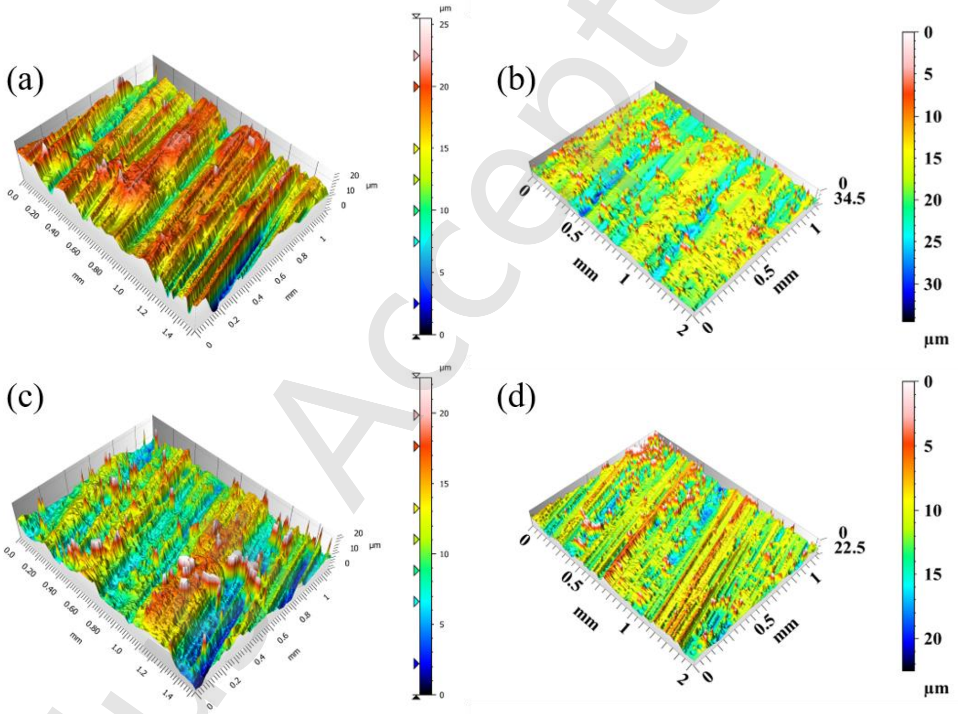

Figure. C2. 3D surface measurement topography of the specimens before and after friction. (a) 3D surface measurement topography before friction; (b) 3D surface measurement topography after friction under the $200N$ normal load; (c) 3D surface measurement topography before friction; (d) 3D surface measurement topography after friction under the $400N$ normal load.

Fig. C3 shows the comparison of power spectral density (PSD) curves before and after friction on a rough metal surface under different normal load conditions. As shown in Fig. C3 (a), under the action of a normal load of $200N$, the PSD curves before and after friction show significant differences in the low-frequency range ($q < 10^{-4}\,\mu m^{-1}$). The PSD value of the pre friction curve is significantly higher than that after friction, indicating that the large-scale surface morphology undergoes significant wear and plastic deformation during the friction process. In the high frequency range ($q > 10^{-4}\,\mu m^{-1}$), the two curves tend to overlap, indicating that small-scale surface features remain relatively stable during friction. Fig. C3 (b) shows a similar trend under a normal force of $400N$, but with higher overall PSD values and more significant differences in the low-frequency range, indicating that increasing the normal load exacerbates the wear of large-scale surface features. This scale dependent wear behavior reveals the selective characteristics of surface morphology evolution during friction processes, providing important evidence for understanding interface contact mechanisms.

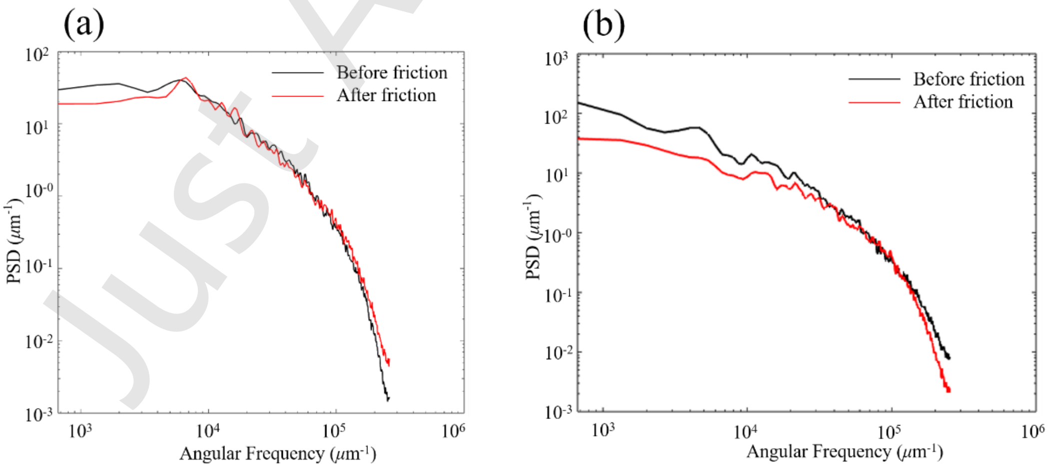

Figure. C3. Comparison of power spectral density before and after friction on rough surfaces under different normal loads: (a) Normal load $200N$; (b) Normal load $400N$.

Acknowledgements

The authors are grateful for the following funding organizations: the Natural Science Foundation of China (grant number 12272157, 12327901), the Natural Science Foundation for Key Program of Gansu Province (grant number 24JRRA782), the Fundamental Research Funds for the Central Universities (grant number lzujbky-2023-ey05).

References

[1] Yan, Y., Chai, M., 2020. Sealing failure and fretting fatigue behavior of fittings induced by pipeline vibration. *Int. J. Fatigue* **136**, 105602. https://doi.org/10.1016/j.ijfatigue.2020.105602

[2] Pradhan, A., Muser, M.H., Miller, N. et al., 2025. The Surface-Topography Challenge: A Multi- ¨ Laboratory Benchmark Study to Advance the Characterization of Topography. *Tribol Lett* 73, 110. https://doi.org/10.1007/s11249-025-02014-y

[3] Lyashenko, I.A.; Pham, T.H.; Popov, V.L., 2024. Pull-Off Strength and Mechanical Energy Dissipation in Adhesive Contacts: Experiments and Simulations. Coatings 14, 188. https://doi.org/10.3390/coatings14020188

[4] Hertz H. Ueber die Berührung fester elastischer Körper.. *Journal für die reine und angewandte Mathematik* 1882;**1882**(92): 156-171. https://doi.org/10.1515/crll.1882.92.156

[5] Greenwood, J. A., Williamson, J. B. P., 1966. Contact of nominally flat surfaces. *Proc. R. Soc. Lond.* A295300–319. http://doi.org/10.1098/rspa.1966.0242

[6] Greenwood, J.A., Tripp, J.H., 1967. The elastic contact of rough spheres. ASME. *J. Appl. Mech*. **34**(1): 153-159. https://doi.org/10.1115/1.3607616

[7] Greenwood, J.A., Tripp, J.H., 1970. The contact of two nominally flat rough surfaces. *P. I. Mech. Eng*. **185**(1): 625-633

[8] Bush, A.W., Gibson, R.D., Thomas, T.R., 1975. The elastic contact of a rough surface. *Wear* **35**(1):87–111. https://doi.org/10.1016/0043-1648(75)90145-3

[9] Majumda,r A., Tien, C. L., 1990. Fractal characterization and simulation of rough surfaces. *Wear* **136**: 313-327. https://doi.org/10.1016/0043-1648(90)90154-3

[10] Persson, B.N.J., Bucher, F., Chiaia, B., 2002. Elastic contact between randomly rough surfaces: comparison of theory with numerical results. *Phys. Rev. B* **65**: 184106. https://doi.org/10.1103/PhysRevB.65.184106

[11] Persson, B.N.J., 2002. Adhesion between an elastic body and a randomly rough hard surface. Eur. *Phys. J. E* **8**, 385–401 (2002). https://doi.org/10.1140/epje/i2002-10025-1

[12] Persson, B.N.J., Albohr, O., Creton, C., Peveri, V., 2004. Contact area between a viscoelastic solid and a hard, randomly rough, substrate. *J. Chem. Phys.* **120**(18): 8779-8793. https://doi.org/10.1063/1.1697376

[13] Persson, B.N.J., 2001. Theory of rubber friction and contact mechanics. *J. Chem. Phys*. **115**: 3840-3861. https://doi.org/10.1063/1.1388626.

[14] Holm, R., 1941. Die technische physik der elektrischen kontakte. Berlin: Springer-Verlag.

[15] Kogut, L., Komvopoulos, K., 2004. Electrical contact resistance theory for conductive rough surfaces separated by a thin insulating film. *J. Appl. Phys*. **95**(2): 576-585. https://doi.org/10.1063/1.1629392.

[16] Barber, J.R., 2003. Bounds on the electrical resistance between contacting elastic rough bodies. *Proc. R. Soc. Lond*. A.45953–66. http://doi.org/10.1098/rspa.2002.1038.

[17] Timsit R.S., 1999. Electrical contact resistance: properties of stationary interfaces. *IEEE Trans. Compon. Packag. Technol.* **22**, 85–98. https://doi.org/10.1109/6144.759357.

[18] Nakamura, M., Minowa, I., 1986. Computer Simulation for the Conductance of a Contact Interface. *IEEE Trans. Comp., Hybrids, Manufact. Technol.* **9**(2): 150-155. https://doi.org/10.1109/TCHMT.1986.1136639.

[19] Minowa, I., Nakamura, M., Kanno, M., 1986. Conductance of A Contact Interface Depending on the Location and Distribution of Conducting Spots. *Proceedings of the Electrical Contacts, Electromechanical Components and Their Application Conference*, 19-28.

[20] Boyer, L., 2001. Contact resistance calculations: generalizations of Greenwood's formula including interface films. *IEEE Trans. Compon. Packag. Technol.* 24, 50–58. https://doi.org/10.1109/6144.910802.

[21] Malucci, R. D., 1990. Multispot Model of Contacts Based on Surface-Features. *Proceedings of the 36th IEEE Holm Conference on Electrical Contacts and 15th International Conference on Electric Contacts* 625-634. https://doi.org/10.1109/HOLM.1990.113069.

[22] Ta, W., Qiu, S., Wang, Y., Yuan, J., Gao, Y., Zhou, Y., 2021. Volumetric contact theory to electrical contact between random rough surfaces. *Tribol. Int.* **160**, 107007. https://doi.org/10.1016/j.triboint.2021.107007.

[23] Zhao, H., Ta, W., Zhou, Y., 2023. The mechanical-thermal-electrical contact behaviors between rough surfaces under cyclic loading. *Acta Mech. Sin.* **39**(10): 123212. https://doi.org/10.1007/s10409-023-23212-x

[24] Wang, K., Su, B., Ta, W., Zhou, Y., 2024. Electro-mechanical contact behavior of rough surfaces in extreme temperature. *Tribol. Int.* **192**: 109306. https://doi.org/10.1016/j.triboint.2024.109306

[25] Wang D, Xu J, Wang F, et al., 2025. A comprehensive review on the fretting wear of electrical contact interface. *Friction*, **13**(8): 9441012. https://doi.org/10.26599/FRICT.2025.9441012

[26] Gao, Z., Fu, W., Wang, W., 2019. Normal contact damping model of mechanical interface considering asperity shoulder-to-shoulder contact and interaction. *Acta. Mech.* **230**: 2413-2424. https://doi.org/10.1007/s00707-019-02392-0.

[27] Jiang x, Pan f, Shao g, et al., 2019. Prediction of electrical contact endurance subject to micro-slip wear using friction energy dissipation approach. *Friction*, **7**(6): 537-550. https://doi.org/10.1007/s40544-018-0230-x

[28] Li, L., Wang, J., Shi, X., Ma, S., Cai, A., 2021. Contact stiffness model of joint surface considering continuous smooth characteristics and asperity interaction. *Tribol. Lett.* **69**: 1-12. https://doi.org/10.1007/s11249-021-01417-x.

[29] Xu, Y., Scheibert, J., Gadegaard, N., Mulvihill, D. M., 2022. An asperity-based statistical model for the adhesive friction of elastic nominally flat rough contact interfaces. *J. Mech. Phys. Solids* **164**: 104878. https://doi.org/10.1016/j.jmps.2022.104878

[30] Ma T, Yu Z, Song A, et al., 2023. Intermittent failure mechanism and stabilization of microscale electrical contact. *Friction*, **11**(4): 538-545. https://doi.org/10.1007/s40544-022-0613-x

[31] Cai Z., Li C., You L., et al., 2024. Prediction of contact resistance of electrical contact wear using different machine learning algorithms. *Friction*, **12**(6): 1250-1271. https://doi.org/10.1007/s40544-023-0810-2

[32] Rezvanian, O., Brown, C., Zikry, M. A., Kingon, A. I., Krim, J., Irving, D. L., & Brenner, D. W., 2008. The role of creep in the time-dependent resistance of Ohmic gold contacts in radio frequency microelectromechanical system devices. *J. Appl. Phys.* **104**(2). https://doi.org/10.1063/1.2953072.

[33] Rezvanian O, Zikry M A, Brown C, et al., 2007. Surface roughness, asperity contact and gold RF MEMS switch behavior. *J Micromech Microeng*, **17**(10): 2006. https://doi.org/10.1088/0960-1317/17/10/012

Wurui Ta. He received his Ph.D degrees in college of civil engineering and mechanics of Lanzhou University, China, in 2016. He is the deputy dean of the Department of mechanics and Engineering Sciences. His research areas cover the superconducting electromagnetic solid mechanics and contact friction mechanics.

Xueqi Zhang. He has been studying for a master's degree in college of civil engineering and mechanics of Lanzhou University since 2023, and his research direction is interface contact and friction behavior.